Chemistry of Metals and Alloys

Chem. Met. Alloys 14 (2021) 17-24
Ivan Franko National University of Lviv
www.chemetal-journal.org

Component interaction in the ternary system Lu–Fe–Sn at 670 K

L. ROMAKA[1]*, V.V. ROMAKA[2], Yu. STADNYK[1], I. ROMANIV[1]

[1] *Department of Inorganic Chemistry, Ivan Franko National University of Lviv, Kyryla i Mefodiya St. 6, 79005 Lviv, Ukraine*
[2] *Anorganische Chemie I, Technische Universität Dresden, Bergstrasse 66, 01069 Dresden, Germany*
* *Corresponding author. E-mail: lyubov.romaka@gmail.com*

Received April 30, 2021; accepted June 30, 2021; available on-line December 1, 2021
https://doi.org/10.30970/cma14.0415

The phase equilibria in the Lu–Fe–Sn ternary system were determined at 670 K in the whole concentration range, using X-ray diffraction, scanning electron microscopy and energy-dispersive spectrometry. The Lu-Fe-Sn system is characterized by the existence of three ternary compounds at 670 K, $LuFe_6Sn_6$ ($MgFe_6Ge_6$-type, space group *P*6/*mmm*, *a* = 0.53741(6), *c* = 0.8875(1) nm), $Lu_5Fe_6Sn_{18}$ ($Tb_4(Tb_{0.6}Sn_{0.4})Rh_6Sn_{18}$-type, space group *Fm*-3*m*, *a* = 1.35324(5) nm), and $Lu_{117}Fe_{52}Sn_{112}$ ($Tb_{117}Fe_{52}Ge_{112}$-type, space group *Fm*-3*m*, *a* = 2.9425(8) nm). An interstitial-type solid solution $LuFe_xSn_2$, based on the binary compound $LuSn_2$ ($ZrSi_2$-type), was found (up to 7 at.% Fe). The solubility of Sn in binary $LuFe_2$ ($MgCu_2$-type) extends up to 5 at.%.

Intermetallics / Phase diagram / Crystal structure / Stannides

1. Introduction

Ternary systems containing a rare-earth metal, iron and a *p*-element attract particular interest, because in such systems, phases that form the base for a new generation of performing permanent magnets, were found, as for example the compound $Nd_2Fe_{14}B$. According to the literature, the phases $R_6Fe_{13}Sn$ ($Pr_6Fe_{13}Ge$-type) and $R_6Fe_{11}Ga_3$ with $La_6Co_{11}Ga_3$ type structures (*R* are Pr, Nd, Sm) are characterized by high temperatures of magnetic ordering (about 400 K) [1,2]. Investigations of the magnetic properties of the RFe_6Ge_6 and RFe_6Sn_6 compounds showed a large variety of magnetic behaviors with rather high ordering temperatures caused by strong Fe-Fe interaction [3]. The magnetic structures of the RFe_6Sn_6 intermetallics, investigated by neutron diffraction and Mössbauer spectroscopy, indicated magnetic ordering of the Fe and rare-earth sublattices at different temperatures [3,4].

R–Fe–Sn phase equilibrium diagrams have already been established for La, Pr, Nd, Sm, Y, Gd, Dy, Ho, and Er [5-13]. Two (*R* = La, Pr, Nd) or three (*R* = Sm) intermediate phases (RFe_xSn_2, $R_6Fe_{13}Sn$, and $SmFe_6Sn_6$) were observed in the systems with light rare earths, whereas for the *R*–Fe–Sn systems where *R* are heavy rare-earth elements, the existence of a single ternary phase, RFe_6Sn_6, crystallizing with various superstructures of the hexagonal YCo_6Ge_6-type, was found. Nevertheless, a complete investigation of the Er–Fe–Sn phase diagram revealed at high Sn content another ternary phase, $Er_5Fe_6Sn_{18}$, with cubic $Tb_4(Tb_{0.6}Sn_{0.4})Rh_6Sn_{18}$-type structure [12]. Studies of the Er–Fe–Sn system at 670 K and 770 K indicated an important influence of the heat treatment on the existence of this ternary phase, which was only found at 670 K [12].

Preliminary information concerning the investigation of the ternary system Lu–Fe–Sn at 870 K (0-49 at.% Sn) and 670 K (more than 50 at.% Sn) was reported in [5]. Three ternary compounds were found: Lu_6Fe_6Sn, $Lu_4Fe_6Sn_{19}$ and ~$Lu_{70}Fe_{15}Sn_{15}$. The crystal structure was determined for $LuFe_6Sn_6$ ($MgFe_6Ge_6$-type). The authors note that $Lu_4Fe_6Sn_{19}$ is a cubic phase with lattice parameter *a* = 1.3537 nm; the crystal structure of the compound of approximate composition $Lu_{70}Fe_{15}Sn_{15}$ was unknown.

To know the intrinsic properties of intermetallics, the first step is to determine their relations with other phases and to evaluate the compositions and homogeneity ranges. This information can be obtained in the process of studying the phase equilibrium diagrams of the corresponding systems, including the influence of heat treatment and atomic size criteria on structural peculiarities and stability of intermediate phases. This knowledge is of great importance for the sample preparation and investigations of the physical properties.

In the present paper we report the isothermal section of the Lu–Fe–Sn ternary system at 670 K,

constructed in the whole concentration range, and structural data of the identified ternary phases.

2. Methods and materials

Samples were prepared using an electric arc furnace by direct arc melting of the constituent elements (overall purity: Lu 99.9 wt.%, Fe 99.99 wt.%, Sn 99.999 wt.%) under a purified argon atmosphere (Ti sponge was used as getter). The buttons were turned over and re-melted twice to ensure the homogeneity. After melting the weight losses did not exceed 1 % of the total mass. Taking into account the low melting temperature of Sn (505 K) and the binary compounds with high Sn content in the Lu–Sn and Fe–Sn systems, an annealing temperature of 670 K was chosen for the investigation of the Lu–Fe–Sn system over the whole concentration range. The alloys were annealed at 670 K for 720 h and then water-quenched. The samples with high Fe content (Fe > 50 at.%) were first annealed at 870 K for two weeks, and at the next step at 670 K for two weeks. Phase analysis was performed using X-ray powder diffraction patterns of the synthesized samples (diffractometer DRON-4.0, Fe *K*α radiation). The observed diffraction intensities were compared with reference powder patterns of the components, binary and known ternary phases (PowderCell program [14]). The elemental and phase compositions of the synthesized samples with an accuracy of ~0.5-1.5 at.% were examined by Scanning Electron Microscopy (SEM) using a Tescan Vega 3 LMU scanning microscope. Quantitative electron probe microanalysis (EPMA) of the samples was carried out by using an energy-dispersive X-ray analyzer with the pure elements as standards (acceleration voltage 20 kV; *K*- and *L*-lines used). At least five measurements were done for each phase in each sample to obtain an average value.

For the crystal structure refinements, XRPD data were collected in the transmission mode on a STOE STADI P diffractometer (linear position-sensitive detector, $2\theta/\omega$-scan; Cu $K\alpha_1$ radiation, curved germanium (1 1 1) monochromator). The crystal structures were refined by the Rietveld method with programs from the FullProf Suite package [15].

A DSC analysis (NETZSCH STA449C Jupiter device) was performed on $Lu_5Fe_6Sn_{18}$ to check the temperature stability. The sample was heated in argon atmosphere up to 870 K at a rate of 10 K/min.

3. Results and discussion

3.1. Binary systems

Data on the phase diagrams of the Lu−Fe, Lu−Sn, and Fe−Sn binary systems, which delimit the ternary Lu−Fe−Sn system, and the structural data of the corresponding binary compounds were taken from the literature [16-18]. In the Fe−Sn system we confirmed the existence of the FeSn and $FeSn_2$ binaries at 670 K in agreement with [16,17]. The other two phases, Fe_3Sn and Fe_3Sn_2, form above 870 K and were not observed at the temperature of investigation. In the Lu−Sn system the three binary phases, Lu_5Sn_3, $LuSn_2$, and Lu_2Sn_5, were confirmed under our conditions, in agreement with the reported phase diagram [16,18]. In addition, the presence of the binary $Lu_{11}Sn_{10}$ [19] was identified by X-ray diffraction and EPMA data.

According to Massalski [16] the Lu−Fe binary phase diagram was investigated above 1070 K and the presence of four binary compounds: Lu_2Fe_{17} (Th_2Ni_{17}-type), Lu_6Fe_{23} (Th_6Mn_{23}-type), $LuFe_2$ ($MgCu_2$-type), and $LuFe_3$ (unknown structure), was reported. To check the existence of the reported binary compounds under our conditions, samples of the corresponding compositions were prepared and annealed at 670 K. The phase analysis of the samples showed the presence of the Lu_2Fe_{17}, Lu_6Fe_{23}, and $LuFe_2$ phases at this temperature. Crystallographic characteristics of the binary compounds of the Lu−Fe, Lu−Sn, and Fe−Sn systems are presented in Table 1. All the binary phases in these systems are characterized by constant compositions.

3.2. Lu-Fe-Sn ternary system

The phase equilibria in the Lu–Fe–Sn system were investigated using X-ray diffraction and (in part) metallographic analyses of 9 binary and 53 ternary alloys. Based on the results, the isothermal section of the Lu–Fe–Sn system was constructed at 670 K over the whole concentration range (Fig. 1). Phase composition and EPMA data of selected alloys are gathered in Table 2, electron microphotographs of some alloys are shown in Fig. 2.

As a result of the investigation of the phase equilibria, the existence of three ternary compounds was established in the Lu–Fe–Sn system at 670 K, crystallographic characteristics of which are given in Table 3. The phase analysis by X-ray diffraction confirmed the existence of the $LuFe_6Sn_6$ stannide with $MgFe_6Ge_6$-type at 670 K [26]. The refined atomic coordinates are: Lu in 1*a* 0 0 0; Fe in 6*i* ½ 0 0.2465(8); Sn1 in 2*c* ⅓ ⅔ 0; Sn2 in 2*d* ⅓ ⅔ ½; Sn3 in 2*e* 0 0 0.3307(7). The refinements of the site occupancies showed that the 1*a* position of the Lu atoms is occupied to 87 %, which was confirmed by EPMA ($Lu_{6.71}Fe_{46.81}Sn_{46.48}$). The data obtained here are in agreement with data reported earlier [26], where deviation from stoichiometry for Lu was determined by neutron diffraction.

At high Sn content the formation of a ternary phase with approximate composition ~$Lu_{15}Fe_{20}Sn_{65}$ was observed, similar to the phase $Lu_4Fe_6Sn_{19}$ [5]. Crystal structure refinements and Mössbauer spectroscopy investigations of this compound have been reported elsewhere [27].

Table 1 Crystallographic characteristics of the Lu–Fe, Lu–Sn and Fe–Sn binary compounds identified at 670 K.

Compound	Structure type	Space group	Lattice parameters, nm			Reference
			a	*b*	*c*	
Lu_2Fe_{17}	Th_2Ni_{17}	*P*6$_3$/*mmc*	0.8338(4)	–	0.8279(5)	this work
Lu_2Fe_{17}	Th_2Ni_{17}	*P*6$_3$/*mmc*	0.8388	–	0.8243	[20]
Lu_6Fe_{23}	Th_6Mn_{23}	*Fm*-3*m*	1.19319(8)	–	–	this work
Lu_6Fe_{23}	Th_6Mn_{23}	*Fm*-3*m*	1.1936	–	–	[20]
$LuFe_2$	$MgCu_2$	*Fd*-3*m*	0.7224(2)	–	–	this work
$LuFe_2$	$MgCu_2$	*Fd*-3*m*	0.7230	–	–	[21]
Lu_5Sn_3	Mn_5Si_3	*P*6$_3$/*mcm*	0.8664(3)	–	0.6346(3)	this work
Lu_5Sn_3	Mn_5Si_3	*P*6$_3$/*mcm*	0.8700	–	0.6355	[22]
$Lu_{11}Sn_{10}$	$Lu_{11}Sn_{10}$	*I*4/*mmm*	1.12953	–	1.6424	[19]
$LuSn_2$	$ZrSi_2$	*Cmcm*	0.4341(2)	1.5974(5)	0.4273(3)	this work
$LuSn_2$	$ZrSi_2$	*Cmcm*	0.4343	1.5997	0.4273	[23]
Lu_2Sn_5	Er_2Ge_5	*Pmmn*	0.4308(3)	0.4388(4)	1.8907(5)	this work
Lu_2Sn_5	Er_2Ge_5	*Pmmn*	0.4292	0.4359	1.8748	[18]
FeSn	CoSn	*P*6/*mmm*	0.5296(4)	–	0.4448(3)	this work
FeSn	CoSn	*P*6/*mmm*	0.5297	–	0.4441	[24]
$FeSn_2$	$CuAl_2$	*I*4/*mcm*	0.6532(3)	–	0.5325(2)	this work
$FeSn_2$	$CuAl_2$	*I*4/*mcm*	0.6526	–	0.5317	[25]

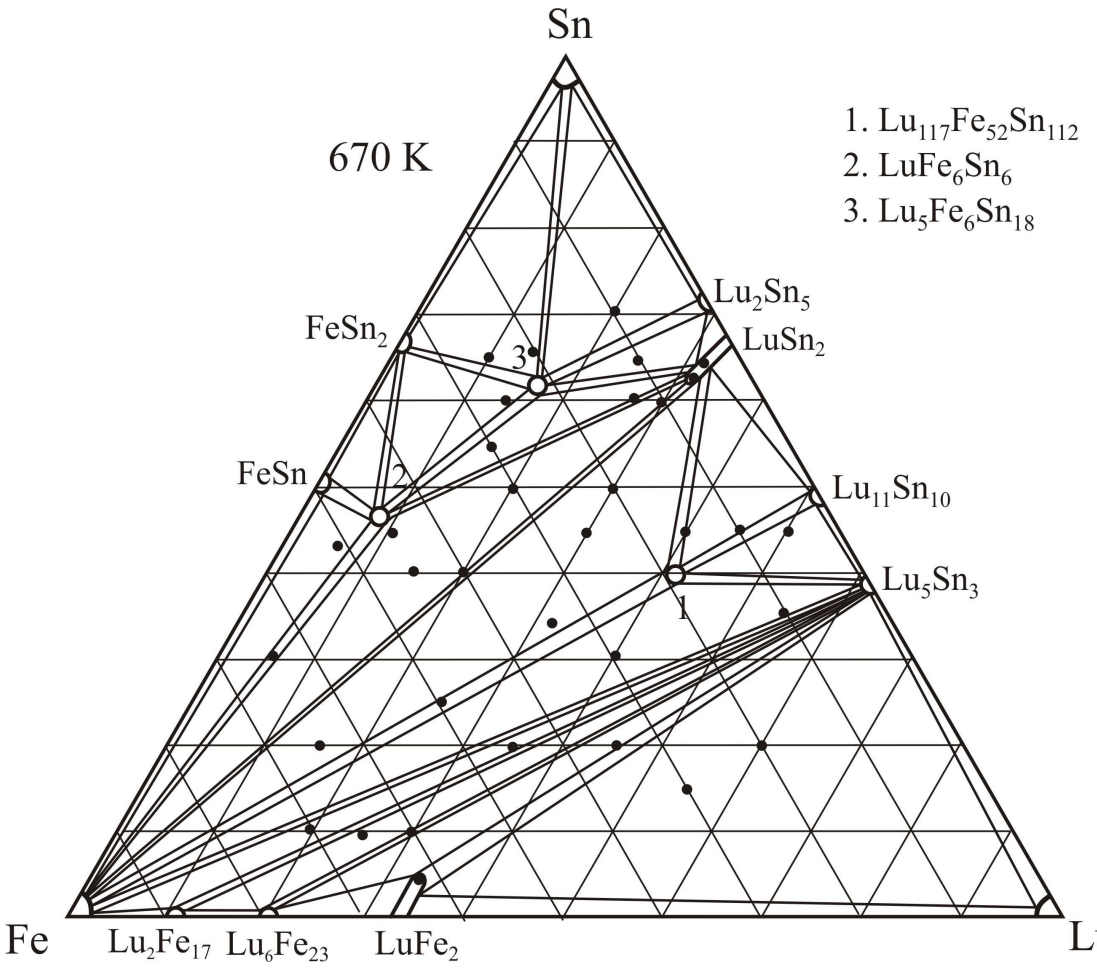

Fig. 1 Isothermal section of the Lu–Fe–Sn system at 670 K.

Table 2 Phase composition, EPMA and crystallographic data for selected Lu–Fe–Sn alloys annealed at 670 K.

Nominal composition	Phase	Structure type	Lattice parameters, nm			EPMA data, at.%		
			a	*b*	*c*	Lu	Fe	Sn
$Lu_{30}Fe_{60}Sn_{10}$	Lu_6Fe_{23}	Th_6Mn_{23}	1.1932(6)	–	–			
	Lu_5Sn_3	Mn_5Si_3	0.8865(2)	–	0.6338(3)			
$Lu_{45}Fe_{35}Sn_{20}$	$LuFe_2$	$MgCu_2$	0.7233(5)	–	–	33.11	61.91	4.98
	Lu_5Sn_3	Mn_5Si_3	0.8666(3)	–	0.6344(4)	62.37	–	37.63
$Lu_{55}Fe_{30}Sn_{15}$	$LuFe_2$	$MgCu_2$	0.7225(4)	–	–	33.21	64.12	2.67
	Lu_5Sn_3	Mn_5Si_3	0.8868(4)	–	0.6436(3)	62.37	–	37.63
	(Lu)	Mg	0.3509(3)	–	0.5566(4)	99.98	–	–
$Lu_{25}Fe_{50}Sn_{25}$	$Lu_{117}Fe_{52}Sn_{112}$	$Tb_{117}Fe_{52}Ge_{112}$	2.9428(6)	–	–	41.14	18.63	40.23
	(α-Fe)	W	0.2874(2)	–	–	–	99.97	–
$Lu_{33}Fe_{33}Sn_{34}$	$Lu_{117}Fe_{52}Sn_{112}$	$Tb_{117}Fe_{52}Ge_{112}$	2.9429(6)	–	–	41.09	18.47	40.44
	$LuFe_xSn_2$	$ZrSi_2$	0.4359(2)	1.6012(2)	0.4298(5)	30.95	6.72	62.33
	(α-Fe)	W	0.2875(2)	–	–	–	99.99	–
$Lu_{40}Fe_{15}Sn_{45}$	$Lu_{117}Fe_{52}Sn_{112}$	$Tb_{117}Fe_{52}Ge_{112}$	2.9427(5)	–	–	41.22	17.98	40.80
	$LuFe_xSn_2$	$ZrSi_2$	0.4347(2)	1.5979(7)	0.4283(2)	32.25	4.01	63.74
$Lu_7Fe_{50}Sn_{43}$	$LuFe_6Sn_6$	$MgFe_6Ge_6$	0.5373(4)	–	0.8875(5)	7.98	46.34	45.68
	(α-Fe)	W	0.2872(3)	–	–	–	99.97	–
	FeSn	CoSn	0.5294(3)	–	0.4446(4)	–	48.38	51.62
$Lu_{10}Fe_{45}Sn_{45}$	$LuFe_6Sn_6$	$MgFe_6Ge_6$	0.5375(4)	–	0.8876(6)	6.88	47.15	45.97
	(α-Fe)	W	0.2872(4)	–	–	–	100.0	–
	$LuFe_xSn_2$	$ZrSi_2$	0.4359(2)	1.6027(6)	0.4298(2)	30.84	6.61	62.55
$Lu_{30}Fe_{25}Sn_{45}$	$Lu_{117}Fe_{52}Sn_{112}$	$Tb_{117}Fe_{52}Ge_{112}$	2.9426(6)	–	–	41.33	18.49	40.18
	$LuFe_xSn_2$	$ZrSi_2$	0.4352(2)	1.5981(5)	0.4288(2)	31.37	5.58	63.05
	(α-Fe)	W	0.2873(3)	–	–	–	99.99	–
$Lu_{45}Fe_{10}Sn_{45}$	$Lu_{117}Fe_{52}Sn_{112}$	$Tb_{117}Fe_{52}Ge_{112}$	2.9426(7)	–	–	41.33	18.49	40.18
	$Lu_{11}Sn_{10}$	$Lu_{11}Sn_{10}$	Not determined			51.59		48.41
$Lu_{30}Fe_{20}Sn_{50}$	$Lu_{117}Fe_{52}Sn_{112}$	$Tb_{117}Fe_{52}Ge_{112}$	2.9427(7)	–	–	41.41	18.56	40.03
	(α-Fe)	W	0.2873(2)	–	–	–	100.0	–
	$LuFe_xSn_2$	$ZrSi_2$	0.4351(3)	1.5993(5)	0.4290(3)	32.91	5.87	61.22
$Lu_{20}Fe_{30}Sn_{50}$	$LuFe_xSn_2$	$ZrSi_2$	0.4360(4)	1.6016(4)	0.4295(1)	30.77	6.86	62.37
	$LuFe_6Sn_6$	$MgFe_6Ge_6$	0.5376(5)	–	0.8874(6)	6.98	46.64	46.38
	(α-Fe)	W	0.2872(4)	–	–	–	100.0	–
$Lu_{15}Fe_{30}Sn_{55}$	$LuFe_6Sn_6$	$MgFe_6Ge_6$	0.5377(5)	–	0.8874(6)			
	$Lu_5Fe_6Sn_{18}$	$Tb_5Rh_6Sn_{18}$	1.3533(3)	–	–			
	$LuFe_xSn_2$	$ZrSi_2$	0.4352(3)	1.5990(7)	0.4291(3)			
$Lu_{30}Fe_{10}Sn_{60}$	$LuFe_xSn_2$	$ZrSi_2$	0.4351(4)	1.5992(8)	0.4291(2)			
	$LuFe_6Sn_6$	$MgFe_6Ge_6$	0.5374(5)	–	0.8875(6)			
	(α-Fe)	W	0.2872(2)	–	–			
$Lu_{15}Fe_{20}Sn_{65}$	$Lu_5Fe_6Sn_{18}$	$Tb_5Rh_6Sn_{18}$	1.3532(2)	–	–	17.58	20.53	61.89
	$FeSn_2$	$CuAl_2$	0.6531(4)	–	0.5319(3)	–	33.27	66.73
	(Sn)		0.5833(2)	–	0.3182(1)	–	–	100.0

We have established that this compound belongs to the cubic $Tb_4(Tb_{0.6}Sn_{0.4})Rh_6Sn_{18}$-type ($Tb_5Rh_6Sn_{18}$, so-called phase II', space group *Fm*-3*m*) [28] and has the formula $Lu_5Fe_6Sn_{18}$. The composition of this phase was confirmed by EPMA, $Lu_{17.57}Fe_{19.61}Sn_{62.82}$. The X-ray diffraction pattern of the $Lu_{15}Fe_{20}Sn_{65}$ sample indicated three phases in equilibrium. The main phase is a ternary tin-rich stannide, $Lu_5Fe_6Sn_{18}$, and the additional phases are $FeSn_2$ ($CuAl_2$-type) and *β*-Sn (Fig. 3). For the $Lu_5Fe_6Sn_{18}$ compound full occupation of the 4*a* position exclusively by Lu atoms was found, in contrast to the type-defining compound $Tb_4(Tb_{0.6}Sn_{0.4})Rh_6Sn_{18}$, where a statistical occupation of the 4*a* site by terbium and tin atoms was observed.

Analysis of the microstructures of the alloys showed that the sample $Lu_{15}Fe_{25}Sn_{60}$, in addition to the three phases in equilibrium, contained traces of tin (white precipitates) (see Fig. 2c). For samples with a high tin content this is due to the low melting point of tin.

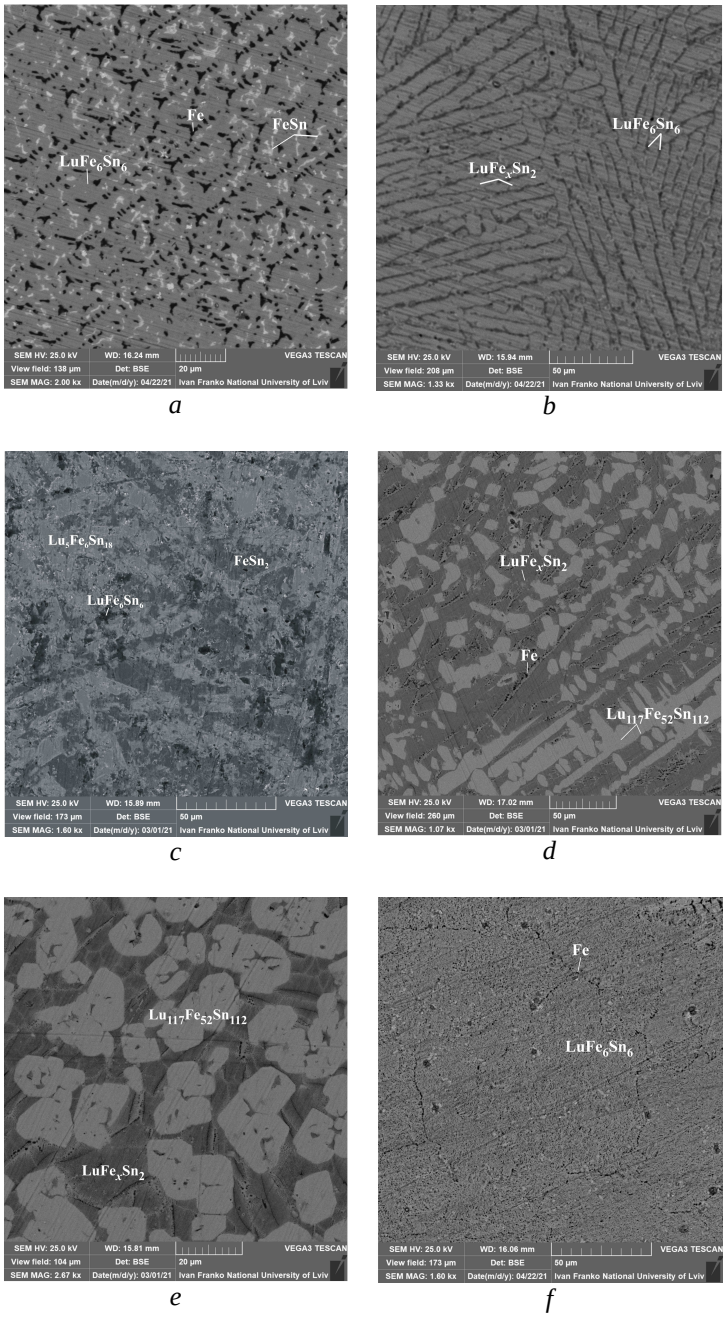

Fig. 2 Microphotographs of selected Lu–Fe–Sn alloys: a) $Lu_7Fe_{50}Sn_{43}$ – $LuFe_6Sn_6$, FeSn, Fe; b) $Lu_{27}Fe_{13}Sn_{60}$ – $LuFe_xSn_2$, $LuFe_6Sn_6$; c) $Lu_{15}Fe_{25}Sn_{60}$ – $FeSn_2$, $Lu_5Fe_6Sn_{18}$, $LuFe_6Sn_6$; d) $Lu_{30}Fe_{20}Sn_{50}$ – $Lu_{117}Fe_{52}Sn_{112}$, $LuFe_xSn_2$, Fe; e) $Lu_{40}Fe_{15}Sn_{45}$ – $Lu_{117}Fe_{52}Sn_{112}$, $LuFe_xSn_2$; f) $Lu_5Fe_{65}Sn_{30}$ – $LuFe_6Sn_6$, Fe.

Table 3 Crystallographic characteristics of the ternary compounds in the Lu–Fe–Sn system. The compound number corresponds to the phase diagram in Fig. 1.

No	Compound	Space group	Structure type	Lattice parameters, nm		
				a	*b*	*c*
1	$Lu_{117}Fe_{52}Sn_{112}$	*Fm*-3*m*	$Tb_{117}Fe_{52}Ge_{112}$	2.9425(8)	–	–
2	$LuFe_6Sn_6$	*P6/mmm*	$MgFe_6Ge_6$	0.53741(6)	–	0.8875(1)
3	$Lu_5Fe_6Sn_{18}$	*Fm*-3*m*	$Tb_4(Tb_{0.6}Sn_{0.4})Rh_6Sn_{18}$	1.35324(3)	–	–

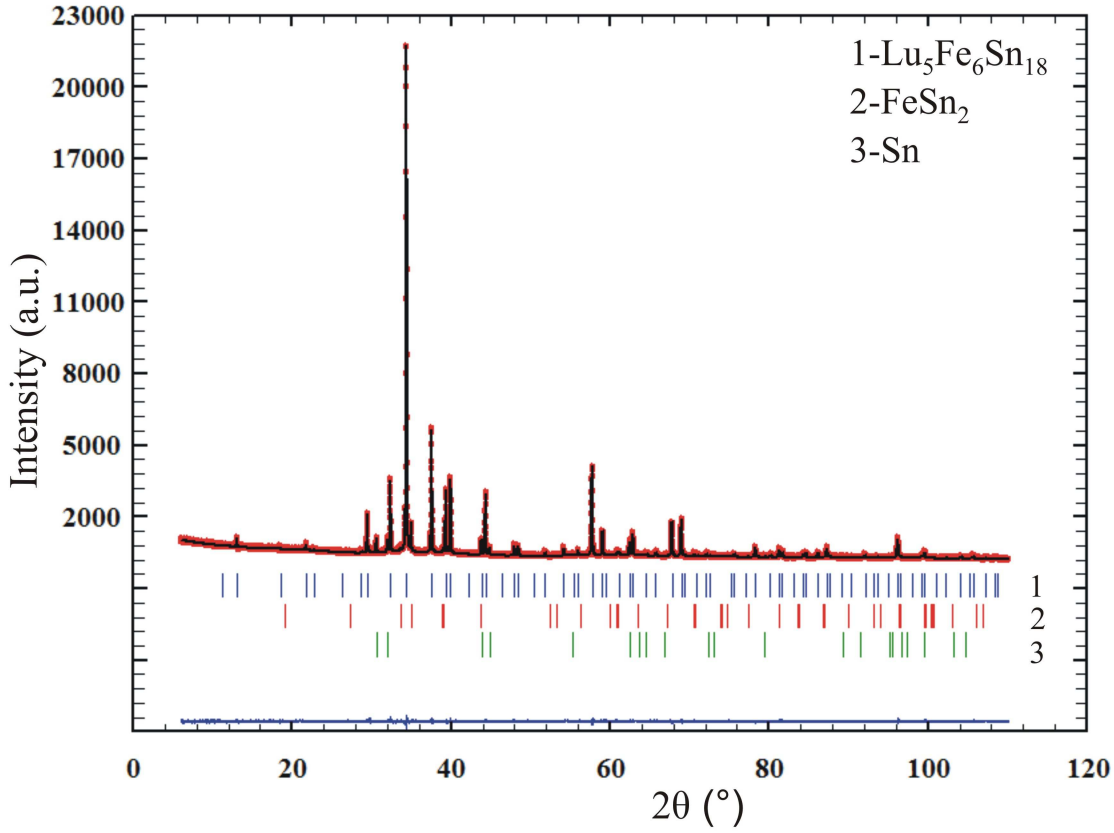

Fig. 3 Experimental (circles), calculated (line), and difference (bottom) X-ray diffraction patterns for $Lu_{15}Fe_{20}Sn_{65}$ sample.

Table 4 Main interatomic distances in $Lu_5Fe_6Sn_{18}$.

Atom	δ, nm	Atom	δ, nm
Fe-Sn2	0.2593	Lu2-Sn3	0.2739
Fe-Sn1	0.2715	Lu2-Sn1	0.3133
Fe-Lu1	0.2964	Lu2-Sn2	0.3167
Lu1-Sn2	0.3311	Sn1-Sn1	0.2444

The analysis of the interatomic distances in the $Lu_5Fe_6Sn_{18}$ compound (Table 4) showed that the distances Fe-Sn2, Fe-Sn1, Sn1-Sn1, and Lu2-Sn3 are shorter than the sum of the respective atomic radii, which may be caused by partial occupation of the sites Lu2, Sn1, and Sn2 and a contribution of covalence to the bond. The structure of $Tb_5Rh_6Sn_{18}$ is characterized by analogous shortening of interatomic distances between Rh and Sn, and Tb and Sn atoms.

With regard to the low melting temperature of Sn and high Sn content (62 at.%), the $Lu_5Fe_6Sn_{18}$ compound was checked using differential scanning calorimetric analysis (NETZSCH STA449C Jupiter device). It was established that the compound is stable up to ~820 K; above this temperature it decomposes.

In the course of our work, a new ternary compound with approximate composition $Lu_{40}Fe_{20}Sn_{40}$ was established. Analysis of the X-ray diffraction pattern of the $Lu_{40}Fe_{20}Sn_{40}$ sample and the calculated lattice parameter indicated that the new compound belongs to the cubic structure type $Tb_{117}Fe_{52}Ge_{112}$. The formation and composition of the $Lu_{117}Fe_{52}Sn_{112}$ compound were confirmed by EPMA data ($Lu_{41.59}Fe_{17.86}Sn_{40.55}$). Microstructure analysis of samples at close compositions showed that $Lu_{117}Fe_{52}Sn_{112}$ is in equilibrium with Fe, $LuFe_xSn_2$ (see Fig. 2d), and the binaries $Lu_{11}Sn_{10}$ or Lu_5Sn_3. As seen from Fig. 2a, the rounded grains of the phase $Lu_{117}Fe_{52}Sn_{112}$ form at the beginning of the crystallization of the $Lu_{40}Fe_{20}Sn_{40}$ alloy. The area around the rounded grains corresponds to the phase $LuFe_xSn_2$ obtained by a peritectic reaction.

To check the formation of the ternary phase ~$Lu_{70}Fe_{15}Sn_{15}$, reported earlier [5], a sample with the

corresponding composition was prepared and annealed separately at 670 K and 870 K. Powder XRD and EPM analyses of the samples annealed at both temperatures revealed that the $Lu_{70}Fe_{15}Sn_{15}$ alloy belonged to the three-phase field involving the binary phases $LuFe_2$, Lu_5Sn_3, and Lu (see Fig. 1).

An interstitial solid solution $LuFe_xSn_2$, based on the binary compound $LuSn_2$ ($ZrSi_2$-type), was observed up to ~7 at.% Fe (a = 0.4352(3), b = 1.5992(6), c = 0.4290(2) nm for composition $Lu_{31}Fe_7Sn_{62}$). As expected, an increase of the volume of the unit cell with increasing Fe content (V = 0.2967 nm^3 for $LuSn_2$, V = 0.2986 nm^3 for $Lu_{31}Fe_7Sn_{62}$) was observed, which confirms the insertion-type of the solid solution. The solubility of Sn in the binary compound $LuFe_2$ ($MgCu_2$-type) is equal to ~5 at.% (a = 0.7235(1) nm for $Lu_{33}Fe_{62}Sn_5$ sample). No significant solubility of the third component in the other binary compounds was observed under the conditions used in our work.

Analysis of the Lu–Fe–Sn system investigated in our work and the {Y, Gd, Dy, Ho, Er}–Fe–Sn systems studied previously showed an influence of the relative atomic size of the rare earths (filling of the *f*-level) on the interaction between the components. Going from Y, Gd, Dy, Ho to Er and Lu the number of ternary compounds increases (from one ternary compound in the {Y, Gd, Dy, Ho}–Fe–Sn system [9-11] to 2 and 3 compounds in the Er–Fe–Sn [12] and Lu–Fe-Sn systems, respectively). For all of the studied *R*–Fe–Sn systems, where *R* is a heavy rare-earth element, the existence of RFe_6Sn_6 ternary phases was found. Depending on the rare-earth element and annealing temperature, the RFe_6Sn_6 stannides crystallize in the hexagonal structure types YCo_6Ge_6, or $MgFe_6Ge_6$, or various superstructures of the YCo_6Ge_6-type. Interstitial-type solid solutions RFe_xSn_2 based on the RSn_2 binary compounds with $ZrSi_2$ structure type are formed in all the studied *R*–Fe–Sn systems, where *R* is a rare earth of the yttrium group.

Among *R*–*M*–Sn systems, where *M* is 3*d*-metal, ternary RM_xSn_y intermetallic phases with high Sn content were known only with Co. The $R_5Fe_6Sn_{18}$ stannides (*R* = Er, Tm, Lu) are new representatives of the RM_xSn_y family with iron. The RM_xSn_y phases, which are characterized by five types of crystal structure (phases I, II, III, V, VII), were analyzed and discussed in detail by Skolozdra [5]. Particular features of these phases are the mixture of rare-earth and tin atoms in one of the crystallographic positions, and the presence of metallic and covalent bonding. On the contrary, the $R_5Fe_6Sn_{18}$ stannides are characterized by full occupation of the 4*a* position by *R* atoms.

Conclusions

The interaction of lutetium with iron and tin at 670 K results in the formation of three ternary compounds: $LuFe_6Sn_6$ ($MgFe_6Ge_6$-type), $Lu_5Fe_6Sn_{18}$ ($Tb_4(Tb_{0.6}Sn_{0.4})Rh_6Sn_{18}$-type), and $Lu_{117}Fe_{52}Sn_{112}$ ($Tb_{117}Fe_{52}Ge_{112}$-type). All the ternary compounds are characterized by a point composition. $Lu_{117}Fe_{52}Sn_{112}$ is a new representative of the $Tb_{117}Fe_{52}Ge_{112}$ structure type with a giant unit cell in the *R*-Fe-Sn systems. At 670 K the solid solubility of the third components in the binary phases is generally limited to 1-2 at.%, except for the $LuSn_2$ and $LuFe_2$ binaries. The formation of interstitial solid solutions based on the RSn_2 binary compounds with $ZrSi_2$-type structure is a common feature of the most of the studied *R*–*M*–Sn systems (*R* = rare earth of the yttrium subgroup, *M* = Fe, Co, Ni). In the Lu–Fe–Sn system the phase relations are relatively complex in the ranges that involve the binary phases of the Lu–Fe system. No ternary compounds were observed in the ternary part with high Fe content; consequently the ternary phases $LuFe_6Sn_6$, $Lu_{117}Fe_{52}Sn_{112}$, and $LuFe_xSn_2$ are in equilibrium with iron.

The study of the Lu–Fe–Sn system performed here confirms the influence of the nature and relative size of the *R*-element on the character of the phase relations in the *R*–Fe–Sn systems.

Acknowledgements

We would like to acknowledge financial support of the Ministry of Education and Science of Ukraine under Grant No. 0121U109766.

References

[1] F. Weitzer, A. Leithe-Jasper, P. Rogl, K. Hiebl, H. Noel, G. Wiesinger, *J. Solid State Chem.* 104 (1993) 368-376. https://doi.org/10.1006/jssc.1993.1172

[2] H. Li, B. Hu, J.M. Cadogan, J.M.D. Coey, J.P. Gavigan, *J. Appl. Phys.* 67 (1990) 4841-4843. https://doi.org/10.1063/1.344754

[3] J.M. Cadogan, D.H. Ryan, *J. Alloys Compd.* 326 (2001) 166-173. https://doi.org/10.1016/S0925-8388(01)01242-7

[4] J.M. Cadogan, D.H. Ryan, O. Moze, Suharyana, M. Hofmann, *J. Phys.: Condens. Matter* 15 (2003) 1757-1772. https://doi.org/10.1088/0953-8984/15/10/322

[5] R.V. Skolozdra, in: K.A. Gschneidner, Jr., L. Eyring (Eds.), *Handbook on the Physics and Chemistry of Rare-Earths*, Vol. 24, North-Holland, Amsterdam, 1997, Ch. 164.

[6] J. Stepien-Damm, O.I. Bodak, B.D. Belan, E. Galdeska, *J. Alloys Compd.* 298 (2000) 169-172. https://doi.org/10.1016/S0925-8388(99)00625-8

[7] P. Salamakha, P. Demchenko, O. Sologub, O. Bodak, J. Stepien-Damm, *Polish J. Chem.* 71 (1997) 305-308.

[8] J. Stepien-Damm, E. Galdeska, O.I. Bodak, B.D. Belan, *J. Alloys Compd.* 298 (2000) 26-29. https://doi.org/10.1016/S0925-8388(99)00626-X
[9] Ya. Mudryk, L. Romaka, Yu. Stadnyk, O. Bodak, D. Fruchart, *J. Alloys Compd.* 383 (2004) 162-165. https://doi.org/10.1016/j.jallcom.2004.04.040
[10] L.C.J. Pereira, D.P. Rojas, J.C. Waerenborgh, *J. Alloys Compd.* 396 (2005) 108-113. https://doi.org/10.1016/j.jallcom.2004.11.061
[11] L. Romaka, Yu. Stadnyk, V.V. Romaka, A. Horpenyuk, *Phys. Chem. Solid State* 21(2) (2020) 272-278. https://doi.org/10.15330/pcss.21.2.272-278
[12] L. Romaka, V.V. Romaka, P. Demchenko, R. Serkiz, *J. Alloys Compd*. 507 (2010) 67-71. https://doi.org/10.1016/j.jallcom.2010.07.137
[13] V.V. Romaka, L.P. Romaka, V.Ya. Krajovskyj, Yu.V. Stadnyk, *Stannides of rare earth and transition metals*, Lviv Polytech. Univ. 2015, 221 p.
[14] W. Kraus, G. Nolze, POWDER CELL – a program for the representation and manipulation of crystal structures and calculation of the resulting X-ray powder patterns, *J. Appl. Crystallogr*. 29, 301 (1996). https://doi.org/10.1107/S0021889895014920
[15] T. Roisnel, J. Rodriguez-Carvajal, WinPLOTR: a Windows tool for powder diffraction patterns analysis, *Mater. Sci. Forum* 378-381 (2001) 118-123. https://doi.org/10.4028/www.scientific.net/MSF.378-381.118
[16] T.B. Massalski, in: *Binary Alloy Phase Diagrams*, American Society for Metals, Metals Park, Ohio, 1990.
[17] H. Okamoto, *Desk Handbook: Phase Diagrams for Binary Alloys*, American Society for Metals, Materials Park, Ohio, 2000.
[18] A. Palenzona, P. Manfrinetti, *J. Alloys Compd.* 201 (1993) 43-47. https://doi.org/10.1016/0925-8388(93)90859-L
[19] C.Y. Yue, F.X. Zhou, M.F. Wang, H.P. Zhang, X.W. Lei, *Chin. J. Struct. Chem.* 32 (2013) 857-862.
[20] F. Liu, W.Q. Ao, L. Pan, Q. Wang, J. Yan, J. Li, *Phase Transitions* 86 (2013) 585-597. https://doi.org/10.1080/01411594.2012.698741
[21] S. Barth, E. Albert, G. Heiduk, A. Möslang, A. Weidinger, E. Recknagel, K.H.J. Buschow, *Phys. Rev. B: Condens. Matter* 33 (1986) 430-436. https://doi.org/10.1103/PhysRevB.33.430
[22] W. Jeitschko, E. Parthé, *Acta Crystallogr.* 22 (1967) 551-555. https://doi.org/10.1107/S0365110X67001112
[23] A. Jandelli, A. Palenzona, G.B. Bonino, *Atti Accad. Naz. Lincei* 40 (1966) 623-628.
[24] K. Brzakalik, *Acta Phys. Pol. A* 114 (2008) 1529-1536.
[25] J.C. Savidan, J.M. Joubert, C. Toffolon Masclet, *Intermetallics* 18 (2010) 2224-2228. http://10.1016/j.intermet.2010.07.007
[26] T. Mazet, B. Malaman, *J. Magn. Magn. Mater.* 219 (2000) 33-40. https://doi.org/10.1016/S0304-8853(00)00415-7
[27] I. Shcherba, L. Romaka, A. Skoblik, B. Kuzel, H. Noga, L. Bekenov, Yu. Stadnyk, P. Demchenko, A. Horyn, *Acta Phys. Pol. A* 136 (2019) 158-163. https://doi.org/10.12693/APhysPolA.136.158
[28] S. Miraglia, J.L. Hodeau, F. De Bergevin, M. Marezio, G.P. Espinosa, *Acta Crystallogr. B* 43 (1987) 76-83. https://doi.org/10.1107/S0108768187098276